NUCL SCI TECH (2016) 27:115
DOI 10.1007/s41365-016-0105-7

Soller slits automatic focusing method for multi-element fluorescence detector

Ya-Yun Yang[1,2] · Qian Gao[1] · Song-Qi Gu[1] · Hai-Sheng Yu[1] · Rui-You Lu[1,2] · Yu-Ying Huang[1]

Received: 28 January 2016 / Revised: 18 April 2016 / Accepted: 19 April 2016 / Published online: 27 August 2016

Abstract In X-ray absorption fine structure (XAFS) experiments, Soller slits are widely used as filter devices in order to improve the signal to noise ratio. Performing high accuracy manual focusing operations is a time-consuming process; therefore, this work introduces an automatic focusing method for Soller slits in multi-element fluorescence detectors. This method establishes a relation model between the fluorescence intensity distribution and the coordinates of the fluorescence excitation point. According to this relation model, the actual coordinates of the fluorescence excitation point can be deduced from the detected fluorescence intensity distribution and used in focusing operations. This method has proven to be feasible in an XAFS experiment at the BL14W1 beamline of the Shanghai Synchrotron Radiation Facility.

Keywords Soller slits · Least square fitting method · Multi-element fluorescence detector · X-ray absorption fine structure

1 Introduction

X-ray absorption fine structure (XAFS) spectroscopy [1] is one of the most powerful tools for depicting the local geometric and electronic structures of matter. The XAFS spectra of low-content samples are usually measured in fluorescence mode. As the common filter device for XAFS experiments, Soller slits [2–6] are used together with 32-element Ge solid-state fluorescence detector [7] in the BL14W1 beamline at Shanghai Synchrotron Radiation Facility (SSRF) [8].

Soller slits are designed with duplicating blades that absorb all or most of the incident fluorescence that does not follow the blades' light paths. According to research by Brian Bewer, in order to obtain the maximum efficiency of Soller slits [9–11], the fluorescence excitation point should be placed at the position of the focal point. It is difficult to obtain high accuracy by manual focusing operations, in which case, we need to develop a system that can implement automatic focusing operations for Soller slits.

This work establishes the relationship between the position of the fluorescence excitation point and the fluorescence intensity distribution, and we provide a method for the automatic focusing of Soller slits: first, calculate the position of the excitation point by fitting the fluorescence intensity distribution, and second, move the excitation point to the focal point in order to achieve the maximum efficiency of the Soller slits. This method has proven to be feasible at the BL14W1 beamline of the SSRF.

2 Theoretical model

2.1 Structure of Soller slits

A view of Soller slits used in the BL14W1 beamline is shown in Fig. 1a. The slits are composed of two groups of blades that consist of 36 optical paths. These paths are focused on the focal point of the Soller slits, and the outlets of these paths correspond to the 32 detection units on the

This work was supported by National Nature Science Foundation of China (No. 11175244).

✉ Qian Gao
gaoqian@sinap.ac.cn

[1] Shanghai Institute of Applied Physics, Chinese Academy of Sciences, Shanghai 201204, China

[2] University of Chinese Academy of Sciences, Beijing 100049, China

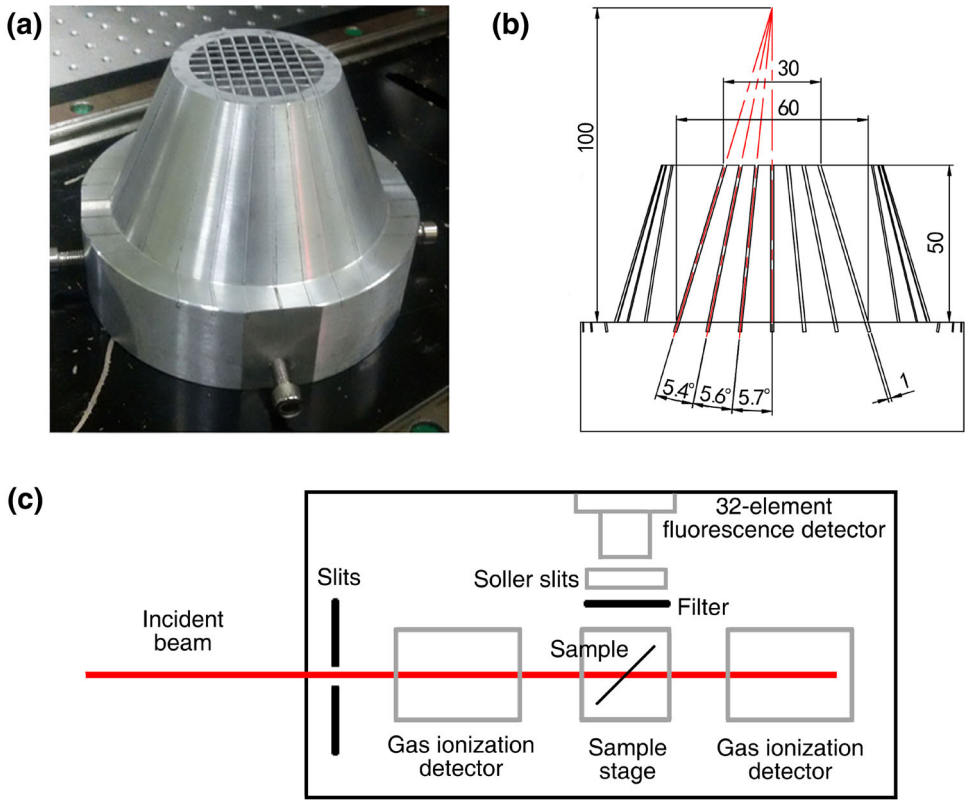

Fig. 1 **a** View of the Soller slits used in the BL14W1 beamline. **b** Design diagram of Soller slits in BL14W1 beamline. **c** Schematic diagram of the XAFS experimental setup in BL14W1 beamline

detector section. Figure 1b shows the two-dimensional design diagram of the Soller slits. The blades are made of aluminum, and each blade has a thickness of 1 mm. The Soller slits have a fixed focal length of 100 mm, a height of 50 mm, an entrance width of 30 mm and an outlet width of 60 mm. Each detection unit has a diameter of 8 mm, and the distance between two detection units' center is 10 mm. Therefore, the angle between two blades on one side is 5.7°, 5.6° and 5.4° from near to far.

2.2 Use of Soller slits in BL14W1 beamline

The BL14W1 beamline is based on a 38-pole wiggler with a maximum magnetic field of 1.2 T. The maximum photon flux at the sample position is about 5×10^{12} photons/s at 10 keV. Currently, BL14W1 is operated in two modes: (1) focusing mode, in which the X-ray goes through the focusing mirror and other optical devices in order to reach the sample position with a spot size of <0.3 mm × 0.3 mm; (2) unfocused mode, in which the X-ray reaches the sample position with a maximum spot size of 40 mm × 4 mm [8]. We recommend using the method provided in this paper under the focusing mode in which the influence of the spot size is small. Figure 1c shows a schematic diagram of the XAFS experiment with a 32-element fluorescence detector. The Soller slits are placed between the filter and the detector. The sample is placed on a computer-controlled sample stage that performs vertical and horizontal translations with micrometer precision. The excitation point should be placed at the position of the focal point once focusing is accomplished. This movement could be implemented with horizontal translations of the sample stage and vertical, horizontal translations of the detector.

2.3 Model of fluorescence intensity distribution

Figure 2 shows the two-dimensional structure and the three-dimensional structure of the Soller slits. The fluorescence excitation point is F', the focal point is F, the number of blades is given by N, the entrance width is D, the detector section width is B, the slit height is H, and the focal length is L.

Set the central point of the detector section as the origin of the coordinate, the detector plane as the X-axis, the focal axis as the Z-axis and build a rectangular coordinate system. The end points of blades can be established as follows

$$d_n = \frac{2n - N - 1}{2(N-1)} D, \tag{1}$$

$$b_n = \frac{2n - N - 1}{2(N-1)} B, \tag{2}$$

where n is the blade number, d_n is the entrance coordinate and b_n is the coordinate of the outlet on the detector section. Assuming that the coordinates of the excitation points

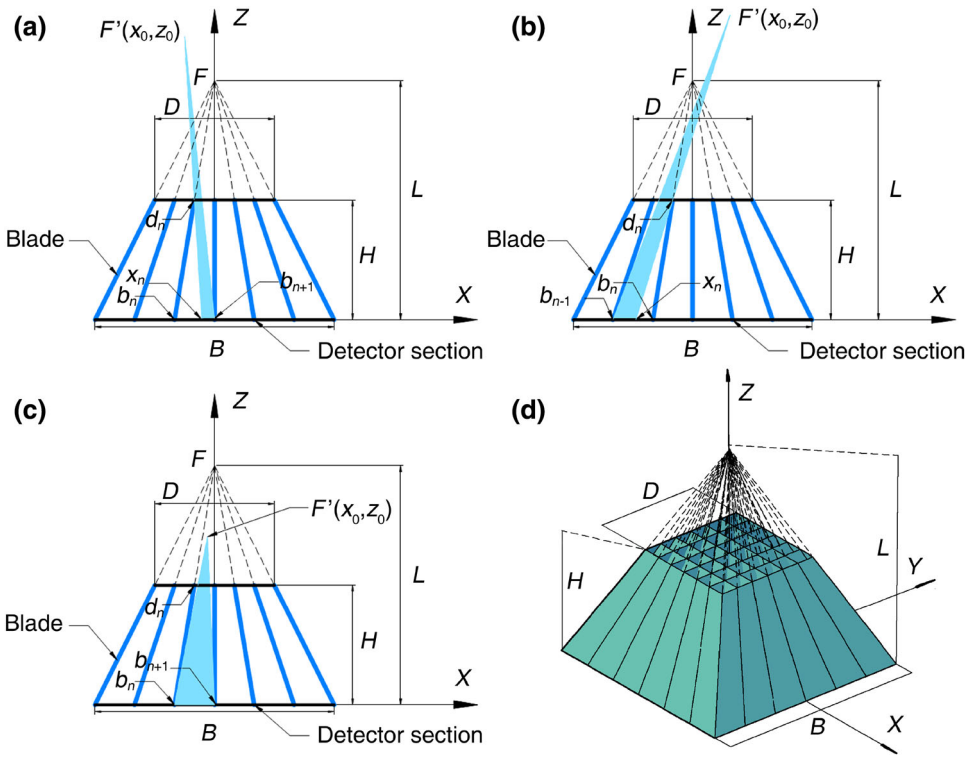

Fig. 2 Structure of Soller slits in two-dimensional space and three-dimensional space. **a**–**c** are three different situations in two-dimensional space. **a** Shows the case when the excitation point F' is on the left side of the focal point F, **b** shows the case when F' is on the right side of F, **c** shows the case when F is above F', the *blue lines* are the blades of the Soller slits, and the pale *blue* area shows the cover of fluorescence in Soller slits under different conditions. **d** Shows the structure of Soller slits in three-dimensional space. (Color figure online)

are (x_0, z_0), the linear equations of the excitation point F' (x_0, z_0) to the entrance end points (d_n, H) are formed as follows

$$z = (z_0 - H)\frac{x - x_0}{x_0 - \frac{2n-N-1}{2(n-1)}D} + z_0. \tag{3}$$

The intersection of the line and the detector section is obtained thusly

$$x_n = \frac{(2n - N - 1)Dz_0 - 2(N - 1)Hx_0}{2(N - 1)(z_0 - H)}. \tag{4}$$

The detector section covered by passed photons is considered as the effective region. Because the fluorescence has a probability distribution in the 4π angle range and the acceptance angle of each channel is small, the fluorescence intensity on the two-dimensional plane can be approximated by the length of the effective region in each channel.

As shown in Fig. 2, (a) if $x_n \geq b_n$ and $x_{n+1} \geq b_{n+1}$ (Fig. 2a), then the effective region of the No. n channel on the detector section is $[x_n, b_{n+1}]$. (b) If $x_n \leq b_n$ and $x_{n+1} \leq b_{n+1}$ (Fig. 2b), then the effective region of the No. n channel is $[b_n, x_{n+1}]$. (c) If $x_n \leq b_n$ and $x_{n+1} \geq b_{n+1}$ (Fig. 2c), then the effective region of the No. n channel is $[b_n, b_{n+1}]$. If $z_0 > L$, then there are only two cases, (a) and (b).

According to Eqs. (2) and (4), the effective region width (f_n) in different cases is obtained using the following methods:

Case (a)

$$f_n = x_{n+1} - b_n = \frac{-2[(B - D)z_0 - BH]n + [(N + 1)B - (N - 1)D]z_0 - 2(N - 1)Hx_0 - (N + 1)BH}{2(N - 1)(z_0 - H)}, \tag{5}$$

Case (b)

$$f_n = b_{n+1} - x_n = \frac{2[(B - D)z_0 - BH]n - [(N - 1)B - (N + 1)D]z_0 + 2(N - 1)Hx_0 + (N - 1)BH}{2(N - 1)(z_0 - H)}, \tag{6}$$

Case (c)

$$f_n = b_{n+1} - b_n = \frac{2(z_0 - H)B}{2(N-1)(z_0 - H)}. \tag{7}$$

In cases (a) and (b), f_n is inversely proportional to z_0. It is easier to receive the fluorescence signal when z_0 is larger than L. Therefore, by setting $z_0 > L$ as the initial condition, we only need to consider cases (a) and (b).

According to Eqs. (5) and (6), the intensity of each channel on the two-dimensional plane has a $n = c_1$ symmetrical distribution. The analytic formulas can be expressed as follows:

$$f_n = |k(n - c_1)| + c_2, \tag{8}$$

$$k = \frac{2[(B-D)z_0 - BH]}{2(N-1)(z_0 - H)}, \tag{9}$$

$$c_1 = \frac{(B-D)Nz_0 + 2(N-1)Hx_0 + BNH}{2[(B-D)z_0 - BH]}, \tag{10}$$

$$c_2 = \frac{[(B+D)z_0 - BH]}{2(N-1)(z_0 - H)}. \tag{11}$$

Figure 2d shows the three-dimensional structure of the Soller slits. The detector plane is set as plane *XY*, the *X*-axis is parallel to the incident beam direction, the *Y*-axis is perpendicular to the beam direction, and the *Z*-axis is parallel to the focal axis. Three-dimensional fluorescence intensity distribution is the product of the two-dimensional distribution in the x direction and that in the y direction:

$$f = [|k(n_x - c_1)| + c_3] \cdot [|k(n_y - c_2)| + c_3]. \tag{12}$$

Above, n_x and n_y are the numbers of the light paths in two directions, which range from 1 to $N - 1$. Considering the fluorescence excitation probability, the distribution in each dimension should be multiplied by a constant coefficient, Q. Therefore, the intensity distribution in the three-dimensional space should be the following:

$$f = Q^2[|k(n_x - c_1)| + c_3] \cdot [|k(n_y - c_2)| + c_3]. \tag{13}$$

2.4 Calculation of excitation point coordinates

The fluorescence intensity distribution coefficients k, c_1, c_2 and c_3 in Eq. (13) are functions of excitation point coordinates (x_0, y_0, z_0). Q, k, c_1, c_2 and c_3 can be calculated by fitting the actual distribution of fluorescence intensity. Q and k cannot be solved separately, and we can only get their products. Bring Qk, c_1, c_2 and Qc_3 into Eqs. (9) and (11),

$$\frac{Qk}{Qc_3} = \frac{2[(B-D)z_0 - BH]}{(B+D)z_0 - BH}. \tag{14}$$

Then z_0 can be calculated,

$$z_0 = \frac{(Qk - 2Qc_3)BH}{Qk(B+D) - 2Qc_3(B-D)}. \tag{15}$$

According to Eq. (10), x_0 and y_0 can be calculated,

$$x_0 = \frac{(B-D)Nz_0 - BNH - k'c_1}{2(N-1)H}, \tag{16}$$

$$y_0 = \frac{(B-D)Nz_0 - BNH - k'c_2}{2(N-1)H}, \tag{17}$$

$$k' = 2[(B-D)z_0 - BH]. \tag{18}$$

3 Design of automatic focusing system

In this design, use MATLAB to complete the fluorescence intensity distribution fitting and excitation point coordinate calculations. LabVIEW and EPICS were applied to build a user interface and control scripts on Windows and Linux separately.

3.1 Fluorescence signal acquisition

An X-ray Instrumentation Associates (XIA) DXP-XMAP acquisition board is used in the BL14W1 beamline to obtain the detector signal. The board combines computer-controlled analog, digital noise reduction and precision multichannel analysis to produce high quality pulse-height spectra from preamplified solid-state X-ray detector signals [12]. LabVIEW obtains the fluorescence counts through API functions provided by XIA [13]. EPICS [14] obtains the fluorescence counts through the DXP module [15, 16]. The fluorescence intensity distribution information is then sent to a fitting script under the MATLAB Runtime [17].

3.2 Data preprocessing

Fluorescence intensity distribution data need to be preprocessed before fitting. This includes a characteristic peak selection, excluding abnormal data, initial value setting and symbol processing.

Characteristic peak selection involves selecting a characteristic fluorescence peak from the multiple fluorescence peaks as the fitting input data. This requires that the characteristic peak reflects the fluorescence intensity distribution of the remaining fluorescence that passes through the Soller slits in the detector. Generally, an isolated and high-intensity fluorescence peak is selected as a characteristic peak and used in data fitting.

The process of excluding abnormal data involves removing the data with no signal or abnormal counts.

The initial value setting greatly influences the time-consumption of the fitting, and an initial value close to the

actual one should be chosen in order to accelerate the convergence of the function. This design uses the following method to carry out the initial value setting.

Set counts of the channel placed on (n_x, n_y) as $Count(n_x, n_y)$, if the highest point (n_{mx}, n_{my}) of the fluorescence intensity distribution is located in the detection zone, then the initial value ($InitValue$) can be set as follows:

$$InitValue(Qk) = \sqrt[4]{k_{mx}^2 \cdot k_{my}^2}, \tag{19}$$

$$InitValue(c_1) = n_{mx}, \tag{20}$$

$$InitValue(c_2) = n_{my}, \tag{21}$$

$$InitValue(Qc_3) = \sqrt[2]{Count(n_{mx}, n_{my})}, \tag{22}$$

where k_{mx} (k_{my}) is the slope k of the fluorescence intensity distribution in y (x) direction whose value depends on the position of the highest point (n_{mx}, n_{my}) and is generated by the fitting function polyfit [18].

Symbol processing involves replacing the absolute value in Formula (13) by multiplying a parameter s with a value of $\pm$ 1. According to Formula (9), k is always positive. Therefore, the highest point (n_{mx}, n_{my}) is considered as the demarcation point to set the s. When $n_x < n_{mx}$, s is set as 1; otherwise, it is set as -1. The same consideration applies to the Y-axis. Formula (13) can be rewritten as follows:

$$f = Q^2[s_x k(n_x - c_1) + c_3] \cdot [s_y k(n_y - c_2) + c_3]. \tag{23}$$

3.3 Least squares fitting

This design uses the MATLAB nonlinear least squares fitting function (lsqcurvefit) to fit the fluorescence intensity distribution [19]. Its structure is shown in Eq. (24).

$$\boldsymbol{x} = lsqcurvefit(fun, \boldsymbol{initvalue}, \boldsymbol{xdata}, \boldsymbol{ydata}, \boldsymbol{lb}, \boldsymbol{ub}, \boldsymbol{options}), \tag{24}$$

where ***initvalue*** is the initial value vector of the fitting parameter as determined by Formulas (19)–(22). ***xdata*** and ***ydata*** are the locations of each channel and the corresponding fluorescence counts, respectively; ***lb*** and ***ub*** are the lower bounds and upper bounds, which generally assigned a null value; ***options*** are the fitting options, including the main algorithm, the stop conditions and other parameters; and *fun* is the fitting function. The expression of the function *fun* is shown in Eq. (25).

$$\begin{aligned} fun = {} & times(mtimes(\boldsymbol{a_1}, times(\boldsymbol{x_3}, \boldsymbol{x_1} - \boldsymbol{a_2})) \\ & + \boldsymbol{a_4}, times(mtimes(\boldsymbol{a_1}, \boldsymbol{x_4}), \boldsymbol{x_2} - \boldsymbol{a_3}) + \boldsymbol{a_4}), \end{aligned} \tag{25}$$

where $\boldsymbol{a_1}$, $\boldsymbol{a_2}$, $\boldsymbol{a_3}$ and $\boldsymbol{a_4}$ are parameter vectors to be fitted corresponding to Qk, c_1, c_2 and Qc_3; $\boldsymbol{x_1}$, $\boldsymbol{x_2}$, $\boldsymbol{x_3}$ and $\boldsymbol{x_4}$ are vectors for fitting that correspond to n_x, n_y, s_x and s_y. After setting the proper convergence conditions, we can get a set of optimal Qk, c_1, c_2 and Qc_3 that satisfies the stopping condition.

3.4 Special case

This method cannot be used to fit the data if the highest point (n_{mx}, n_{my}) of the fluorescence intensity distribution falls out of the detection zone. According to the fluorescence intensity distribution model, the fitting function cannot converge in this case. Therefore, the procedure needs to provide approximate coordinates of the excitation point to move (n_{mx}, n_{my}) into the detection zone and then invoke the fitting process. The methods are as follows:

Estimate the distance between the fluorescence excitation point and the detector plane in order to calculate the value of k and c_3 according to Formula (9) and (11). The fitting function can converge to stop conditions if k and c_3 have been calculated. Bring the data into the fitting script in order to obtain an approximate value of c_1 and c_2. Obtain the approximate excitation point coordinates (x_0, y_0) according to Formula (16) and (17). Then move the excitation point to (0, 0, z_{0a}), and make a precise fitting.

3.5 Adjustment of excitation point position

After the fluorescence intensity distribution coefficients have been calculated, the coordinates of the excitation point can be obtained. Figure 3a shows the schematic diagram of the XAFS experimental setup using a multi-element fluorescence detector. The rectangular coordinate system is based on the central point of the detector section. The direction and position of the incident beam will not change, and the distance between the Soller slits and the detector is fixed. Therefore, the coordinates of the excitation point (x_0, y_0, z_0) can only be changed by adjusting the sample and detector positions.

For the X-axis, which is parallel to the X-ray direction, the value of x_0 can be adjusted by moving the sample in the X-ray direction. The distance of the sample stage moving in the X direction is equal to the change value of x_0.

For the Y-axis, which is perpendicular to the X-axis on the detector section plane, the value of y_0 can be adjusted by moving the vertical height of the detector. Because the height of the incident beam is almost not changed, the value of y_0 will not change after the initial adjustment.

For the Z-axis, which is parallel to the focal axis of Soller slits, the value of z_0 can be adjusted by moving the detector in the direction of the focal axis. A change in the Z-axis has less of an effect on the Soller slits' efficiency than a change on the X-axis, so z_0 is adjusted after adjusting x_0.

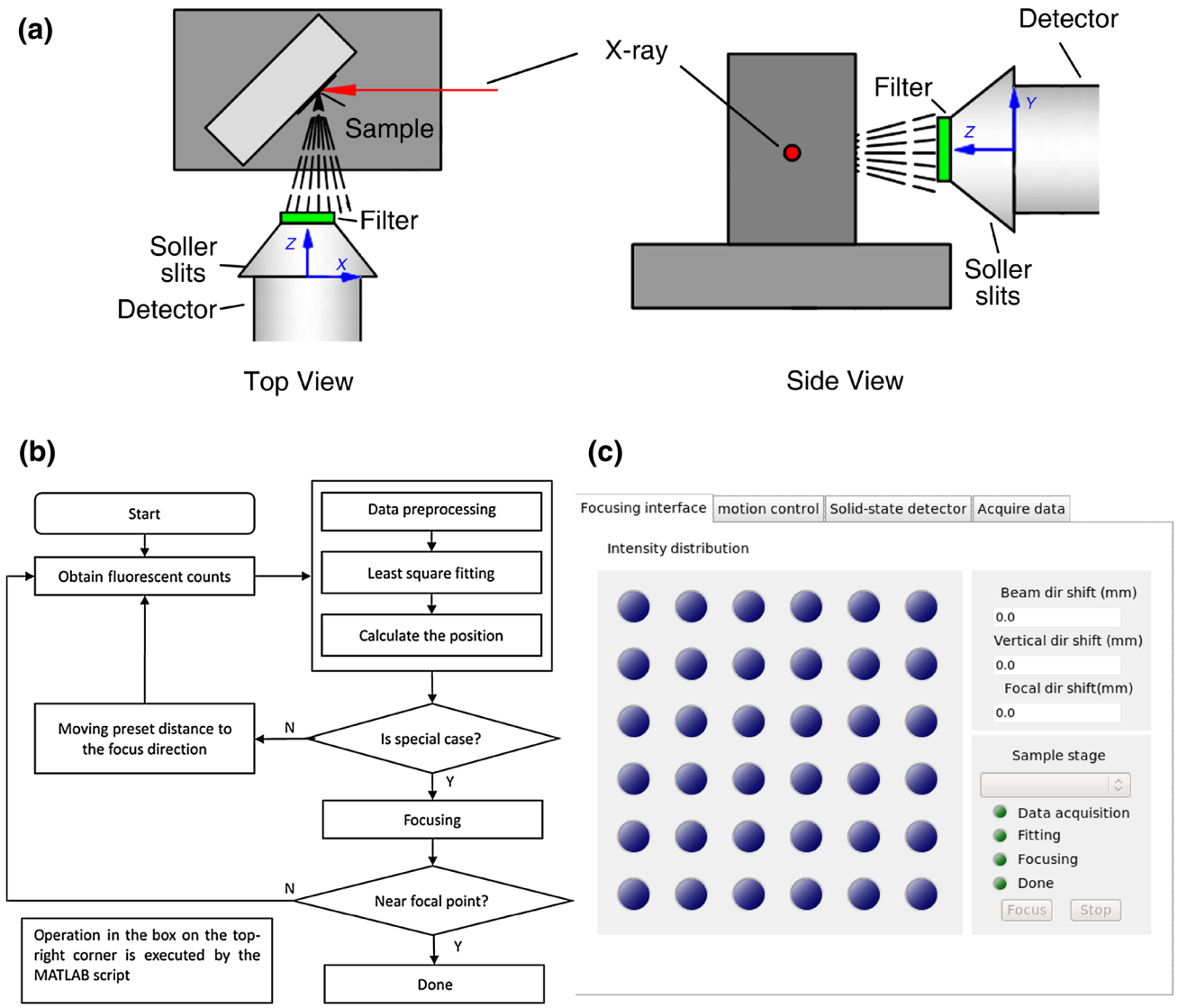

Fig. 3 **a** Schematic diagram of the XAFS experimental setup using multi-element fluorescence detector, **b** the flow chart and **c** graphical user interface

3.6 Flowchart and graphical user interface

The automatic focusing operation of the system is completed using the EPICS/LabVIEW [20]. To ensure focusing accuracy, this procedure should be repeated several times. The program's flow chart is shown in Fig. 3b, and the graphical user interface is shown in Fig. 3c. This source code can be downloaded at https://github.com/ltaskpt/Soller-slits.

4 Results and discussion

4.1 Accuracy of coordinate calculation

Figure 4a shows the contrast between the fitting results in three-dimensional space (multi-color) and the actual fluorescence intensity distribution (blue). This figure suggests that the fitting results accurately reflect the fluorescence distribution. Figure 4b, c shows the goodness of fit between the actual *X*-coordinate of the excitation point and the calculated *X*-coordinate under different *Z* conditions. The excitation point takes 1 mm as the step size when moving along the *X*-axis. These results indicate that the fitting results are linear with the actual data and are highly accurate near the focal point.

4.2 XAFS experiments

Figure 5a, b shows the X-ray fluorescence spectra of copper sulfate solution under different conditions: (a) before the focusing procedure (not focused), and (b) after the procedure (nearly focused). This experiment was

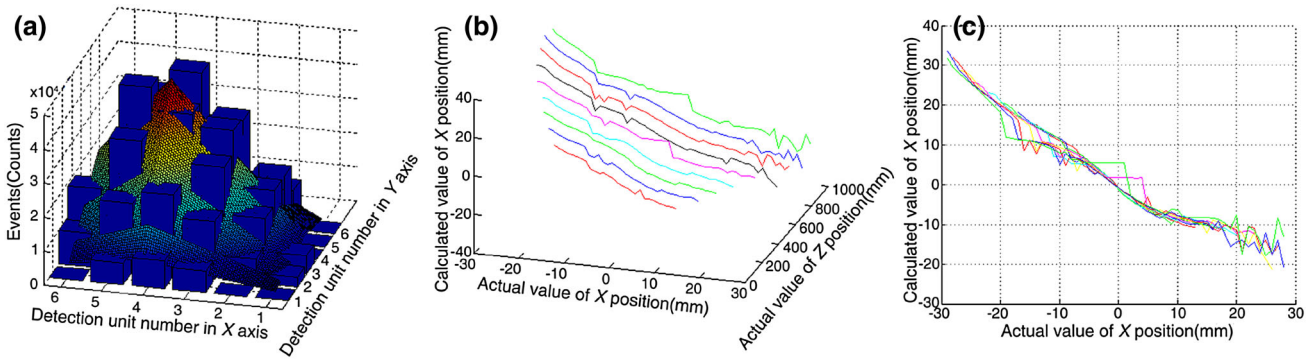

Fig. 4 **a** The contrast between the fitting results in three-dimensional space (*color*) and the actual fluorescence intensity distribution (*blue*). **b** Direct view and **c** front view of the goodness of fit between the calculated X-coordinate and the actual one of the excitation point under different *Z* conditions. (Color figure online)

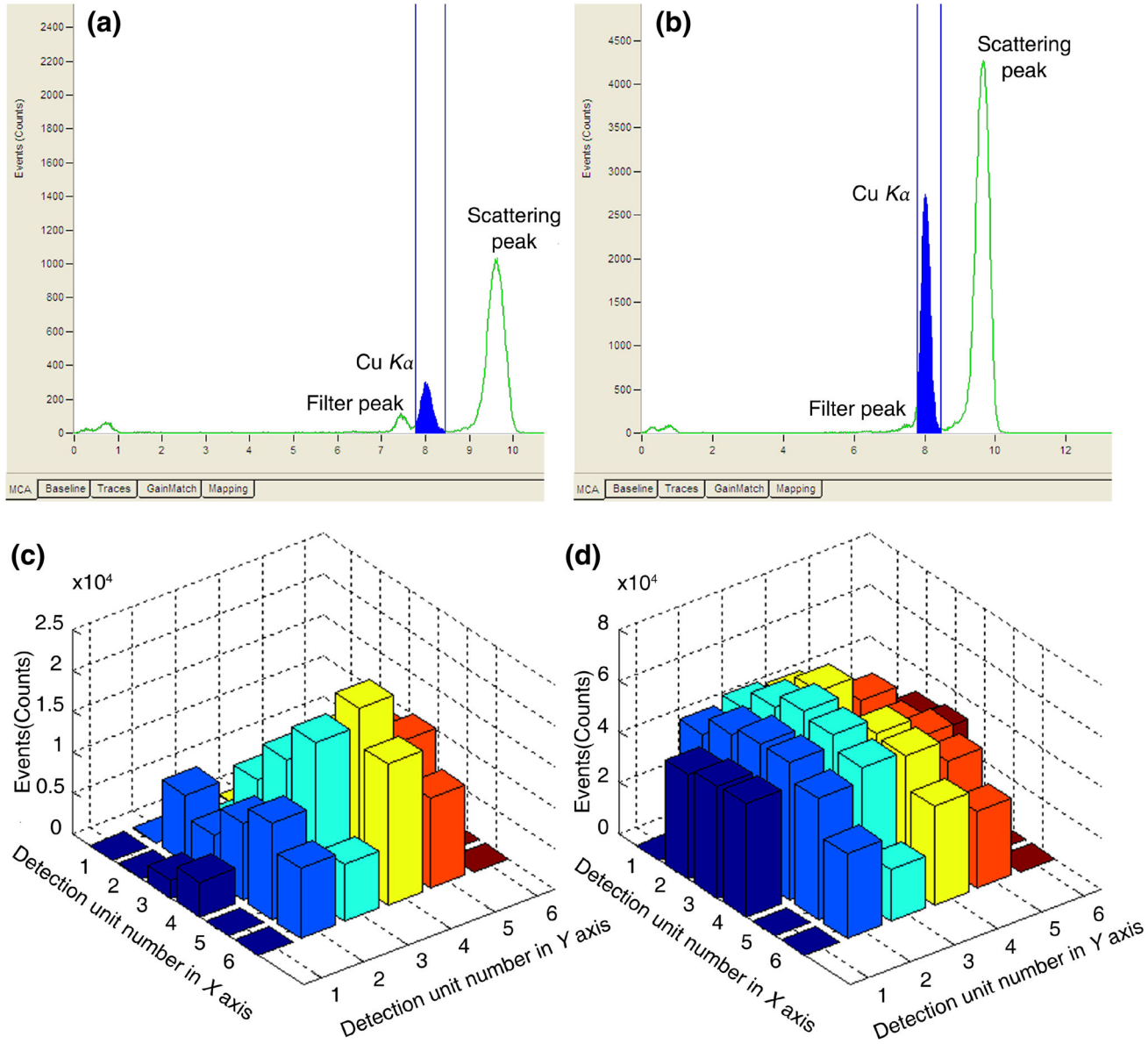

Fig. 5 Spectra with Soller slits **a** not focused, **b** nearly focused. The fluorescence peak covered by *blue* is the target fluorescence peak (8046.3 eV). Target fluorescence intensity distribution **c** before the focusing procedure, **d** after the focusing procedure. (Color figure online)

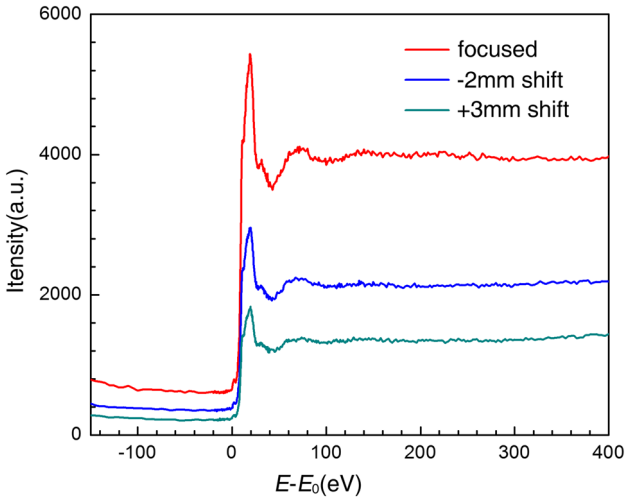

Fig. 6 Three XAFS spectrum at Mn *K*-edge (E_0, 6539 eV) for a solid sample of $MnCl_2$ mixed with LiF. The focused condition demonstrates a higher signal to noise ratio than other two unfocused conditions

conducted under the incident beam-focusing mode. A filter of Ni was placed between the sample and the Soller slits. The $K\alpha$ fluorescence line of Cu (8046.3 eV) was set as the target fluorescence peak, which is covered by blue. This demonstrates that, with focused Soller slits, the target fluorescence intensity is greatly increased compared to the condition when Soller slits are not well focused. Figure 5c, d shows the distribution of the target fluorescence using the focusing system. After the focusing operation, the fluorescence intensity of each unit is greatly improved, and the distribution is more uniform. Because of the small differences between the solid angle of each optical path, the fluorescence counts should be nearly the same in every detection unit when the excitation point is located at the focal point. This suggests that the focusing system can accurately realize automatic focusing for the excitation point.

Figure 6 shows three XAFS spectra at Mn *K*-edge (6539 eV) for a solid sample of $MnCl_2$ well mixed with LiF. The content of Mn is about ten times that of the ppm level. This experiment was conducted under the incident beam-focusing mode. These three spectra were obtained under the conditions of focused Soller slits, a -2 mm shift on the *X*-axis and a $+3$ mm shift on the *X*-axis, separately. Let the signal consist of N_0 fluorescent and N_b background counts per second. The signal to noise ratio, *S/N*, is given by Formula (26), where $A = N_b/N_0$ and τ is the time of measurement [3].

$$\frac{S}{N} = \left(\frac{N_0\tau}{1+A}\right)^{\frac{1}{2}}. \tag{26}$$

Compared to the focused condition, the two unfocused conditions cause fewer decreases in the background (near 37 % at -2 mm shift and 64 % at $+3$ mm shift), and a larger decrease of signal (near 43 % at -2 mm shift and 68 % at $+3$ mm shift) at the same time. Therefore, focused Soller slits will obtain maximum efficiency for increasing the signal to noise ratio, and this work can be realized accurately using the auto focusing system.

5 Conclusion

The use of focusing Soller slits will be beneficial in obtaining maximum detector efficiency, which can improve the signal to noise ratio in fluorescence XAFS experiments. An automatic focusing method for Soller slits used with a multi-element fluorescence detector was introduced. In this method, a relation model between the fluorescence intensity distribution and the coordinates of the fluorescence excitation points was established. According to this relation model, the actual coordinates of the fluorescence excitation points were deduced using MATLAB scripts. The focusing operation was implemented with movements of the sample stage and detector. Non-solvable cases were well handled through the estimating procedure. Experimentation has shown that this method obtains high accuracy and saves time during the focusing process.

References

1. M. Newville, Fundamentals of XAFS. Rev. Mineral. Geochem. **78**, 33–74 (2014). doi:10.2138/rmg.2014.78.2
2. J.J. Tse, G.N. George, I.J. Pickering, Use of Soller slits to remove reference foil fluorescence from transmission spectra. J. Synchrotron Radiat. **18**, 527–529 (2011). doi:10.1107/S090904951100344X
3. E.A. Stern, S.M. Heald, X-ray filter assembly for fluorescence measurements of X-ray absorption fine structure. Rev. Sci. Instrum. **12**, 1579–11582 (1979). doi:10.1063/1.1135763
4. F.W. Lytle, D.E. Sayers, E.A. Stern, Extended X-ray-absorption fine-structure technique. II. Experimental practice and selected results. Phys. Rev. B **11**, 4825–4835 (1975). doi:10.1103/PhysRevB.11.4825
5. E.A. Stern, D.E. Sayers, F.W. Lytle, Extended X-ray-absorption fine-structure technique. III. Determination of physical parameters. Phys. Rev. B **11**, 4836–4846 (1975). doi:10.1103/PhysRevB.11.4836
6. W. Soller, A new precision X-ray spectrometer. Phys. Rev. **24**, 158–167 (1924). doi:10.1103/PhysRev.24.158
7. CANBERRA Industries Inc. Germanium Array Detectors. http://www.canberra.com/products/detectors/germanium-detectors.asp
8. H.S. Yu, X.J. Wei, J. Li et al., The XAFS beamline of SSRF. Nucl. Sci. Technol. **26**, 050102 (2015). doi:10.13538/j.1001-8042/nst.26.050102
9. B. Bewer, Soller slit design and characteristics. J. Synchrotron Radiat. **19**, 185–190 (2012). doi:10.1107/S0909049511052319
10. W.C. Stoecker, J.W. Starbuck, Effect of Soller slits on X-ray intensity in a modern diffractometer. Rev. Sci. Instrum. **36**, 1593–1598 (1965). doi:10.1063/1.1719399

11. T.N. White, An inherent limitation of soller (multiple) slits. Rev. Sci. Instrum. **4**, 590–592 (1933). doi:10.1063/1.1749007
12. Digital X-ray Processor User's Manual (2008), http://www.xia.com/Manuals/XMAP_User_Manual.pdf. Accessed 19 Nov 2008
13. Handel API (2002), http://www.xia.com/Manuals/Handel_API_012902_branch2.PDF. Accessed June 2002
14. J. Jacky, EPICS-based control system for a radiation therapy machine. Paper presented at 14th International Conference on Accelerator & Large Experimental Physics Control Systems (ICALEPCS2013), San Francisco, USA, 6–11 Oct 2013
15. M. Rivers, SynApps: dxp (2015), http://cars.uchicago.edu/software/epics/dxp.html. Accessed 20 Jan 2015
16. D. Zimoch, StreamDevice home page (2014), http://epics.web.psi.ch/software/streamdevice/. Accessed 5 Feb 2014
17. About the MATLAB Runtime (2012), http://www.mathworks.com/help/compiler/about-the-matlab-runtime.html. Accessed March 2012
18. Polyfit (2010), http://www.mathworks.com/help/matlab/ref/polyfit.html. Accessed Sept 2010
19. Lsqcurvefit (2010), http://cn.mathworks.com/help/optim/ug/lsqcurvefit.html. Accessed Sept 2010
20. K. Kasemir, G. Carcassi, Control system studio guide (2015), http://cs-studio.sourceforge.net/docbook. Accessed 12 Oct 2015